Variable-temperature multinuclear solid-state NMR study of oxide ion dynamics in fluorite-type bismuth vanadate and phosphate solid electrolytes

Matthew T. Dunstan,[†,¶] David M. Halat,[†,¶] Matthew L. Tate,[‡] Ivana Radosavljevic Evans,[‡] and Clare P. Grey[*,†]

Department of Chemistry, University of Cambridge, Lensfield Road, Cambridge, CB2 1EW, United Kingdom, and Department of Chemistry, University Science Site, Durham University, South Road, Durham DH1 3LE, United Kingdom

E-mail: cpg27@cam.ac.uk

Abstract

Ionic-conducting materials are crucial for the function of many advanced devices used in a variety of applications, such as fuel cells and gas separation membranes. Many different chemical controls, such as aliovalent doping, have been attempted to stabilise δ-Bi_2O_3, a material with exceptionally high oxide ion conductivity which is unfortunately only stable over a narrow temperature range. In this study, we employ a multinuclear, variable-temperature NMR spectroscopy approach to characterise and measure oxide ionic motion in the V- and P-substituted bismuth oxide materials $Bi_{0.913}V_{0.087}O_{1.587}$, $Bi_{0.852}V_{0.148}O_{1.648}$ and $Bi_{0.852}P_{0.148}O_{1.648}$, previously shown to have excellent ionic conduction properties (Kuang *et al*., *Chem. Mater.* 2012,

[*]To whom correspondence should be addressed

[†]Department of Chemistry, University of Cambridge, Lensfield Road, Cambridge, CB2 1EW, United Kingdom

[‡]Department of Chemistry, University Science Site, Durham University, South Road, Durham DH1 3LE, United Kingdom

[¶]Contributed equally to this work

24, 2162; Kuang *et al.*, *Angew. Chem. Int. Ed.* 2012, *51*, 690). Two main ^{17}O NMR resonances are distinguished for each material, corresponding to O in the Bi–O and V–O/P–O sublattices. Using variable-temperature (VT) measurements ranging from room temperature to 923 K, the ionic motion experienced by these different sites has then been characterised, with coalescence of the two environments in the V-substituted materials clearly indicating a conduction mechanism facilitated by exchange between the two sublattices. The lack of this coalescence in the P-substituted material indicates a different mechanism, confirmed by ^{17}O T_1 (spin-lattice relaxation) NMR experiments to be driven purely by vacancy motion in the Bi–O sublattice. ^{51}V and ^{31}P VT-NMR experiments show high rates of tetrahedral rotation even at room temperature, increasing with heating. An additional VO_4 environment appears in ^{17}O and ^{51}V NMR spectra of the more highly V-substituted $Bi_{0.852}V_{0.148}O_{1.648}$, which we ascribe to differently distorted VO_4 tetrahedral units that disrupt the overall ionic motion, consistent both with linewidth analysis of the ^{17}O VT-NMR spectra and experimental results of Kuang *et al.* showing a lower oxide ionic conductivity in this material compared to $Bi_{0.913}V_{0.087}O_{1.587}$ (*Chem. Mater.* 2012, *24*, 2162). This study shows solid-state NMR is particularly well suited to understanding connections between local structural features and ionic mobility, and can quantify the evolution of oxide-ion dynamics with increasing temperature.

Introduction

Anionic-conducting materials, especially oxide ion conductors, have been the focus of continued research efforts over the past decades due to their potential use in renewable energy applications, such as oxygen-permeable membranes and solid oxide fuel cells (SOFCs).[1–3] A crucial parameter holding back their widespread implementation is the undesirably high temperature at which they show sufficiently high ionic conduction, which even for currently used, best-in-class materials (such as yttria-stabilised zirconia, YSZ) is >923 K.[4] There is still very much a need to discover and develop novel ionic conducting materials that operate at lower temperatures and to characterise the connection between structure and conductivity in order to move towards rational design of

optimal materials.

Bismuth oxides and various substituted derivatives have been mined as a rich compositional space within which to find new fast ion conductors, sparked by the extremely high oxygen ionic conductivity values of the cubic δ phase of Bi_2O_3, which is not stable at lower temperatures due to transformation to a monoclinic polymorph below 1003 K.[5,6] Of the families of materials that have been explored, including phases resulting from isovalent doping (rare earth Ln^{3+})[7–12] as well as aliovalent doping (such as pentavalent P, V, Nb, and/or Ta),[13–22] vanadium-substituted bismuth oxides have shown the most promising values of ionic conductivity at relatively lower temperatures.[23,24] These materials often exhibit complex superstructures; understanding the role the V dopant plays in enabling the superionic behaviour of the Bi–O lattice is correspondingly complex, but is nonetheless necessary in elucidating the best way to optimise these materials for device applications.

In the previous work of Kuang *et al.*, two novel bismuth-rich phases in the $Bi_{1-x}V_xO_{1.5+x}$ system (x = 0.087, 0.095) were found to have high oxide ion conductivity between 573–773 K, competitive with the best-performing Bi_2O_3-based materials currently known.[23] Subsequent studies involving *ab initio* molecular dynamics (AIMD) simulations found that for these materials, as well as a related phase with x = 0.148 (also known as β-$Bi_{46}V_8O_{89}$), distinct structural features, such as variably-coordinated VO_x polyhedra, played key roles in the ionic migration pathways through the material, in particular facilitating oxygen exchange between the polyhedra and the Bi–O sublattice.[24] The structure of the higher-substituted material $Bi_{0.852}V_{0.148}O_{1.648}$ is shown in Figure 1, highlighting the layers containing Bi and O interspersed with layers containing VO_4 polyhedra. This phase can be thought of as having a monoclinic, ordered fluorite superstructure where V^{5+} replaces some of the Bi^{3+} sites in δ-Bi_2O_3, with concomitant reordering of oxygen vacancies to preserve fourfold coordination around the V atoms. Darriet *et al.* reported a very similar structure in the same monoclinic *C*2/*m* space group for the P-substituted analogue $Bi_{0.852}P_{0.148}O_{1.648}$ (also reported as $Bi_{46}P_8O_{89}$), with layers of PO_4 tetrahedra rather than VO_4.[25] At lower doping levels, such as in the x = 0.087 ($Bi_{0.913}V_{0.087}O_{1.587}$) phase, a long-range ordered pseudo-cubic 3 × 3 ×

3 fluorite superstructure is instead adopted. In the more highly substituted, monoclinic phases, the ordering of vacancies and dopants leads to a disruption of the underlying cubic symmetry of the Bi_2O_3 sublattice, which by comparison is essentially maintained in $Bi_{0.913}V_{0.087}O_{1.587}$.

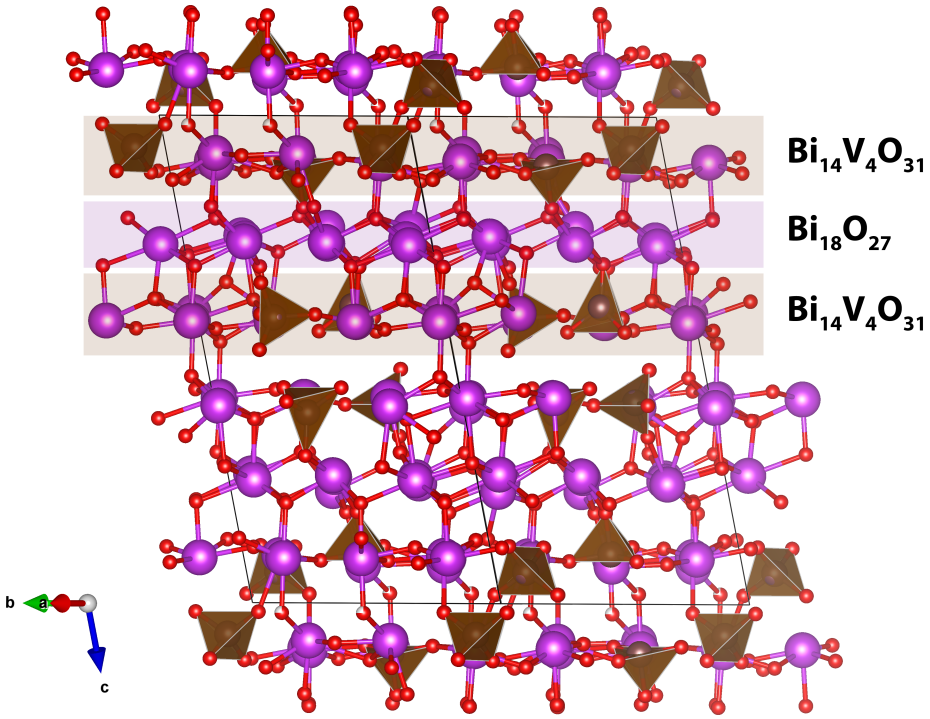

Figure 1: Crystallographic structure of $Bi_{0.852}V_{0.148}O_{1.648}$ (also known as β-$Bi_{46}V_8O_{89}$), shown along the $[1\bar{1}0]$ direction, as reported by Kuang *et al.*[24] Bismuth atoms are shown in purple, oxygen atoms in red, and vanadium atoms (and VO_4 tetrahedral units) in brown. The monoclinic (space group *C*2/*m*) structure comprises a characteristic stacking of two layers containing VO_4 tetrahedra ($Bi_{14}V_4O_{31}$) and one bismuth oxide rock salt layer ($Bi_{18}O_{27}$) containing only OBi_4 units. All VO_4 groups are isolated.

In this work, we report a comprehensive experimental study of the oxide-ion dynamics of both $Bi_{0.913}V_{0.087}O_{1.587}$ and $Bi_{0.852}V_{0.148}O_{1.648}$ using multinuclear variable-temperature solid state nuclear magnetic resonance (VT-NMR), and compare the conduction mechanisms of these phases to the P-substituted analogue $Bi_{0.852}P_{0.148}O_{1.648}$. ^{17}O VT-NMR experiments have previously been shown to be particularly well-suited to the elucidation of ion conduction mechanisms in related materials such as the Aurivillius-type layered α-$Bi_4V_2O_{11}$, γ-$Bi_4V_{1.7}Ti_{0.3}O_{10.85}$[26] and the fluorite-related $Bi_{26}Mo_{10}O_{69}$.[27] These VT-NMR experiments can distinguish amongst crystallographic

oxygen environments present in the phases as well as their corresponding motional processes and rates. In this study, we have used ^{17}O, ^{51}V and ^{31}P NMR to characterise the mechanisms of, and activation energy values for, ionic motion in $Bi_{0.913}V_{0.087}O_{1.587}$, $Bi_{0.852}V_{0.148}O_{1.648}$, and $Bi_{0.852}P_{0.148}O_{1.648}$. We find that oxide-ion exchange between the Bi–O and V–O sublattices occurs with increasing temperature for both $Bi_{0.913}V_{0.087}O_{1.587}$ and $Bi_{0.852}V_{0.148}O_{1.648}$, whereas no evidence of exchange between the sublattices is observed for $Bi_{0.852}P_{0.148}O_{1.648}$. We also find that the concentration of dopant is critical for maximising the rate of conduction, with higher dopant concentrations leading to the formation of VO_x polyhedra that do not participate in ionic conduction pathways and instead hinder the overall movement of oxide ions through the structure. Furthermore, the use of dopant atoms that are unable to support variable O coordination (*e.g.*, P) hinders exchange between the two sublattices; this finding helps to explain previous reports of oxide-ion conductivity about half an order of magnitude lower for the P-substituted phase relative to the β-$Bi_{46}V_8O_{89}$ material over the same temperature range.[24,28]

Experimental Methods

Synthesis and ^{17}O-enrichment

Samples of $Bi_{0.913}V_{0.087}O_{1.587}$, $Bi_{0.852}V_{0.148}O_{1.648}$ and $Bi_{0.852}P_{0.148}O_{1.648}$ were synthesised according to the previous literature.[23,24,28] Polycrystalline samples were synthesised by a conventional solid state route using Bi_2O_3 (99.9%, Sigma-Aldrich), V_2O_5 (99.99%, Sigma-Aldrich) and $(NH_4)H_2PO_4$ ($\geq$98%, Sigma-Aldrich). Stoichiometric quantities of the starting materials were ground under isopropanol and heated at 700 °C, 750 °C, 800 °C and finally at 825 °C (for the vanadates) and 850 °C (for the phosphate), for 12 h at each temperature (using heating and cooling rates of 5 °C/min) with intermediate grinding. Sample purity was confirmed by laboratory powder X-ray diffraction (XRD) carried out with a Bruker D8 Advance diffractometer using Cu Ka radiation, *via* Pawley and Rietveld fitting implemented in Topas Academic software.[29–31] ^{17}O-enriched samples were obtained by heating as-synthesised powders to 900 °C under an atmosphere

of 70% $^{17}O_2$ (Cambridge Isotope Laboratories, USA; used as received) in a Pt crucible inside a sealed quartz tube for 24 h. Samples were cooled slowly from the enrichment temperature to maximise ^{17}O uptake. Sample purity after ^{17}O-enrichment was confirmed using room-temperature X-ray powder diffraction (XRD) data collected on a Panalytical X'Pert Pro diffractometer using Cu K_α radiation (data shown in Supporting Information); the reflections could be indexed to a cubic space group for $Bi_{0.852}V_{0.148}O_{1.648}$, and a monoclinic space group for $Bi_{0.852}P_{0.148}O_{1.648}$ and $Bi_{0.852}V_{0.148}O_{1.648}$.

Solid-state NMR spectroscopy

Solid-state ^{17}O, ^{51}V and ^{31}P magic-angle spinning (MAS) NMR spectra were obtained at 16.4 T on a Bruker Avance III 700 MHz spectrometer operating at a Larmor frequency of 94.95 MHz (^{17}O), 184.05 MHz (^{51}V) and 283.39 MHz (^{31}P); initial room-temperature measurements were performed using a double resonance 1.3 mm Bruker probe, at a MAS rate of 60 kHz, and using a rotor-synchronised spin-echo pulse sequence with a $\pi/2$ excitation pulse length of 1.4 μs (for ^{17}O), with a recycle delay of 50 ms. Variable-temperature measurements from room temperature to 973 K were performed at the same field using a triple resonance 7 mm Bruker laser probe.[32,33] Temperature calibration of the probe was carefully performed by measuring the ^{79}Br resonance of KBr over the entire temperature range,[34] with KBr typically included in the same rotor as the sample as an internal temperature reference. The temperatures given in the text correspond to actual sample temperatures with an estimated accuracy of $\pm$10, 20 and 30 K in the 293–473 K, 473–673 K and 673–873 K temperature ranges, respectively. Samples were packed in 4 mm boron nitride (BN) inserts within 7 mm zirconia rotors, which were subsequently spun at 4 kHz for variable-temperature experiments. One-dimensional experiments were performed with a rotor-synchronised spin-echo pulse sequence, using a 9 μs, 4 μs, or 6.5 μs $\pi/2$ excitation pulse, with recycle delays of 50 ms, 0.5 s, or 30 s (for ^{17}O, ^{51}V, and ^{31}P, respectively). Additional ^{17}O measurements, including relaxation experiments, were obtained at 11.7 T on a Bruker Avance III 500 MHz spectrometer operating at a Larmor frequency of 67.83 MHz, using a double resonance

4 mm Bruker probe at a MAS rate of 12.5 kHz, with an excitation pulse of 2.2 μs (for O^{Bi} sites) or 5.0 μs (for O^{V} sites). Variable-temperature spin-lattice (T_1) relaxation experiments at this field were performed using a standard saturation recovery pulse sequence, with a maximal delay of 2.4 s (for O^{Bi} sites) or 0.24 s (for O^{V} sites). Temperature calibration of this probe was also performed by measuring the ^{79}Br resonance of KBr, with estimated accuracy of $\pm$5 K. Finally, ^{17}O measurements were performed at 4.7 T on a Bruker Avance III 200 MHz spectrometer operating at a Larmor frequency of 27.14 MHz, using a double resonance 1.3 mm Bruker probe at a MAS rate of 40 kHz, with an excitation pulse of 0.5 μs, and a recycle delay of 50 ms; these experiments were performed in order to extract quadrupolar parameters from the field-dependent second-order quadrupolar shift (see Supporting Information for further details). ^{17}O chemical shifts were externally referenced to H_2O at 0 ppm, ^{51}V chemical shifts were externally referenced to NH_4VO_3 at −570 ppm,[35,36] and ^{31}P chemical shifts were externally referenced to H_3PO_4 (aq) at 0 ppm. NMR data were processed with TopSpin 3.2.

Results

^{17}O NMR

Room-temperature ^{17}O MAS NMR spectra of all three materials (Figure 2) were initially obtained with fast MAS (60 kHz) in order to achieve higher resolution. For each spectrum, a number of different oxygen environments can be distinguished with resonances ranging from ∼130–630 ppm. The common feature at 220 ppm is assigned to oxygen within the Bi–O sublattice (O^{Bi}), consistent with this chemical environment occurring in all three structures. Similar ^{17}O chemical shifts of oxygen environments coordinated to Bi have been previously reported, such as in Bi_2O_3[37] (195 ppm), as well as the so-called 'BIMEVOX' systems[26] (250–270 ppm), Bi_2WO_6[38] (242 ppm), and BiM_2PO_6 with M = Cd, Zn (200–250 ppm).[39] In these previous ^{17}O NMR studies of Bi-containing oxides, the local O environment corresponds to OBi_4, with a shift range of 190–270 ppm; we are not aware of ^{17}O shifts reported for OBi_3 sites. The feature at 620 ppm present in both V-

substituted samples is attributed to O in VO_4 tetrahedra (O^V), consistent with the established shift range of O^V environments (600–1000 ppm).[26,40] Finally, the resonance at 130 ppm, present only in spectra of the P-substituted sample, is assigned to O in PO_4 tetrahedra (O^P), with a shift that compares favourably to recent ^{17}O NMR studies of a range of solid inorganic acid phosphates (80–150 ppm).[41,42] A minor peak observed at 140 ppm in both V-substituted samples is tentatively assigned to bismuth silicate (estimated at ∼1 wt.%), which forms by reaction with the quartz vessel during the ^{17}O-enrichment procedure; similar ^{17}O shifts have been reported for other silicates such as glasses and apatite oxide-ion conductors.[43,44]

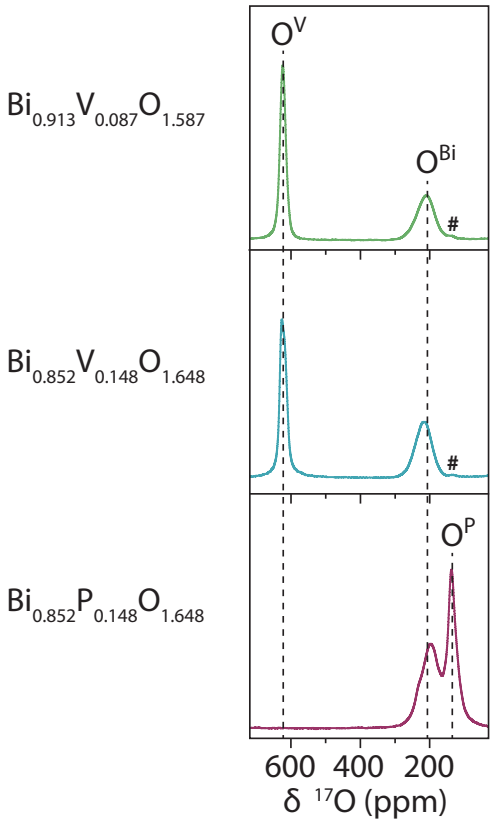

Figure 2: Room temperature ^{17}O MAS NMR spectra of $Bi_{0.852}P_{0.148}O_{1.648}$, $Bi_{0.913}V_{0.087}O_{1.587}$ and $Bi_{0.852}V_{0.148}O_{1.648}$ obtained at 16.4 T at a spinning rate of 60 kHz, with a recycle delay of 50 ms. All three samples show a common feature at ∼220 ppm, assigned to O in the Bi–O sublattice (O^{Bi}), with additional resonances arising from VO_4 and PO_4 environments (O^V and O^P) at ∼620 ppm and ∼130 ppm, respectively. The # symbol denotes the peak at 140 ppm assigned to a minor (∼1 wt. %) bismuth silicate impurity phase.

Representative ^{17}O NMR spectra obtained upon heating all three materials to 823 K are col-

lated in Figure 3; the full datasets are shown in the Supporting Information (SI). The ^{17}O spectra for both V-substituted samples show qualitatively similar behaviour with increasing temperature, and in particular both the O^{V} and O^{Bi} resonances significantly narrow in linewidth up to 573 K. Above 573 K, both resonances disappear for both samples, before reappearing as a single coalesced resonance at 823 K; the shift of this coalesced feature is 332 ppm for $Bi_{0.913}V_{0.087}O_{1.587}$ and 391 ppm for $Bi_{0.852}V_{0.148}O_{1.648}$. This behaviour is indicative of exchange between the two different types of sites occurring on the so-called NMR timescale, where the rate of motion approaches the frequency separation between the two spectral features. Interpolation using the full set of spectra (see SI) allows us to estimate the temperature at which the maximum broadening and initial coalescence is observed, where the rate of ionic motion is directly proportional to the frequency separation. On this basis, we calculate sublattice exchange rates of 87 kHz at 723 K for pseudo-cubic $Bi_{0.913}V_{0.087}O_{1.587}$, and 86 kHz at 748 K for monoclinic $Bi_{0.852}V_{0.148}O_{1.648}$. At comparable temperatures, the motional rate is somewhat slower in the more highly V-substituted, crystallographically lower-symmetry material.

For each phase, the chemical shift of the fully coalesced peak also gives information as to the residence time of mobile O^{2-} ions in O^{Bi} environments vs. O^{V} environments. The coalesced shift of 332 ppm for the $Bi_{0.913}V_{0.087}O_{1.587}$ phase corresponds to a ratio of 70:30 (O^{Bi}:O^{V}), while the shift of 391 ppm for $Bi_{0.852}V_{0.148}O_{1.648}$ gives a ratio of 52:48 (O^{Bi}:O^{V}). This result is intuitively reasonable given the higher concentration of V in $Bi_{0.852}V_{0.148}O_{1.648}$. Furthermore, the expected ratios of O^{Bi}:O^{V} sites calculated from the nominal stoichiometry values, assuming isolated VO_4 tetrahedra, (*i.e.,* 79:21 for $Bi_{0.852}V_{0.148}O_{1.648}$ and 64:36 for $Bi_{0.913}V_{0.087}O_{1.587}$) are significantly larger than the actual ratios calculated from the coalescence data. This result suggests the VT-NMR data are sensitive to the presence of oxygen vacancies in the Bi–O sublattice and/or over-coordination of the VO_4 units. For $Bi_{0.852}V_{0.148}O_{1.648}$, the relative number and/or residence time of O^{V} sites is 33% larger than that expected solely from stoichiometry, whereas it is 43% larger than expected for $Bi_{0.913}V_{0.087}O_{1.587}$, implying that the latter phase has a higher average V coordination. Kuang *et al.* also found from AIMD simulations at 1373 K that the coordination number of V sites

varied between 4.0 and 4.3 for both V-substituted phases, with the larger average coordination number observed for the lower V-substituted material, in excellent agreement with the present results.[23,24]

For $Bi_{0.852}P_{0.148}O_{1.648}$, the temperature-dependent behaviour of the ^{17}O spectra differs significantly from that of the V-substituted samples. With increasing temperature, both the O^P and O^{Bi} resonances exhibit linewidth narrowing that is indicative of increased rates of local oxide-ionic motion, and this narrowing allows for observation of an additional resonance for each environment above ∼473 K. However, even at 873 K, the two groups of resonances remain distinct, showing no sign of the coalescence that is seen in $Bi_{0.913}V_{0.087}O_{1.587}$ and $Bi_{0.852}V_{0.148}O_{1.648}$. This result is indicative of ionic motion that remains local (*e.g.*, PO_4 rotations or librations) or is confined to distinct sublattices, with minimal long-range exchange between the Bi–O and P–O sublattices on the NMR timescale. Moreover, the appearance of spinning sideband intensity arising from the O^P environment (but not from O^{Bi}) above 673 K is suggestive of increasing rates of *local* ionic motion, and further supports the idea that the motion remains distinct between the two sublattices.

Closer examination of the isotropic peaks (*i.e.*, the central transition, or CT, centreband) corresponding to the O^V environments in the ^{17}O spectra of the V-substituted samples shows that, for $Bi_{0.913}V_{0.087}O_{1.587}$, the CT centreband can be fit to a single Voigt function, corresponding to a single type of O^V environment. On the other hand, the fit to the CT centreband for $Bi_{0.852}V_{0.148}O_{1.648}$ requires two such functions with relative intensity varying with temperature (Figure 4), indicating the presence of two distinct types of O^V environments in the more highly V-substituted material. The simple two-peak fits to the O^V features are justified, as the quadrupole coupling constants (C_Q's) of the O^V sites are below 0.9 MHz, and second-order quadrupolar effects are too small to account for the observed lineshapes, including the broad linewidths (see SI). The relatively broad room-temperature linewidths (for the O^V sites for the V-doped samples, and the O^{Bi} sites in general) are likely to arise due to *J*-coupling to the abundant quadrupolar nuclei ^{51}V (I = 7/2) and ^{209}Bi (I = 9/2).

The two types of O^V environments display different temperature-dependent behaviours and

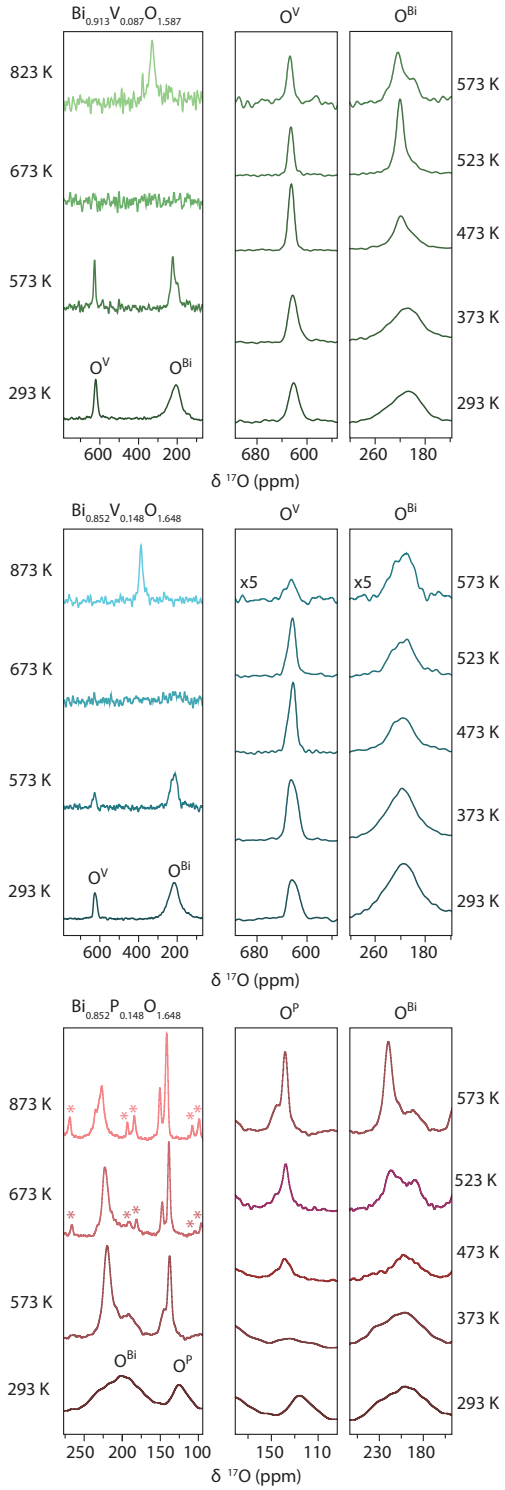

Figure 3: Variable-temperature ^{17}O MAS NMR spectra of $Bi_{0.913}V_{0.087}O_{1.587}$, $Bi_{0.852}V_{0.148}O_{1.648}$ and $Bi_{0.852}P_{0.148}O_{1.648}$ obtained at 16.4 T at a spinning rate of 4 kHz, with a recycle delay of 50 ms. The high-temperature ^{17}O spectra for both V-substituted samples show first the broadening and disappearance (at 673 K) and then the coalescence of the two distinct ^{17}O features above this temperature, indicative of increasingly fast motion between the O^{Bi} and O^{V} environments with increasing temperature. In contrast to the V-substituted samples, for $Bi_{0.852}P_{0.148}O_{1.648}$ no coalescence of the two ^{17}O resonances is observed with increasing temperatures, indicating a minimal rate of O hopping between distinct environments over this temperature range. Spinning sidebands are denoted by asterisks.

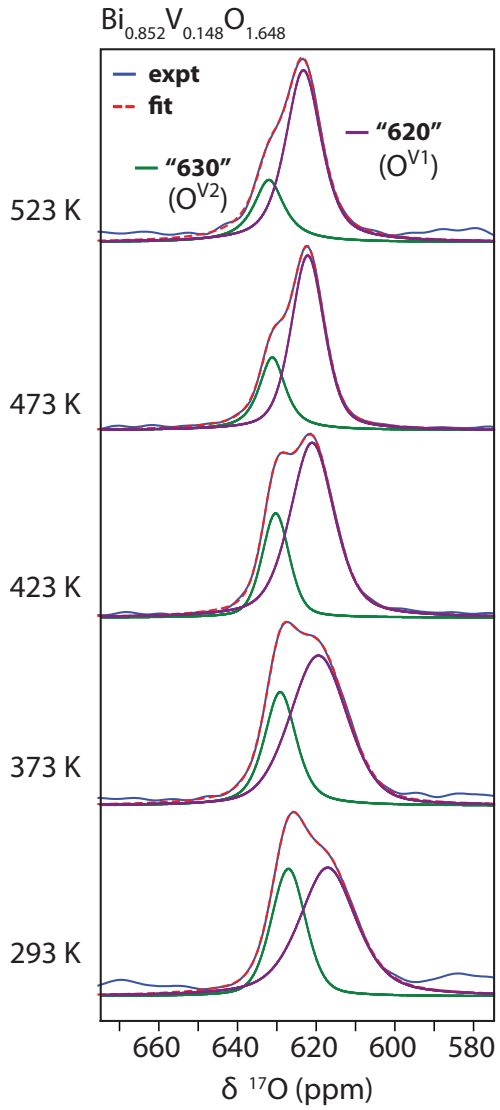

Figure 4: Variable-temperature ^{17}O MAS NMR spectra of $Bi_{0.852}V_{0.148}O_{1.648}$, focusing on the isotropic peaks of the O^V environments, measured at 16.4 T at a spinning rate of 4 kHz from room temperature to 523 K. The O^V resonance in the $Bi_{0.852}V_{0.148}O_{1.648}$ sample comprises two distinct Voigt functions, with relative intensity changing with increasing temperature (compared to the single peak seen in $Bi_{0.913}V_{0.087}O_{1.587}$). Experimental spectra are shown in blue, summed fits in red, and the individual fitted lineshapes in purple and green respectively.

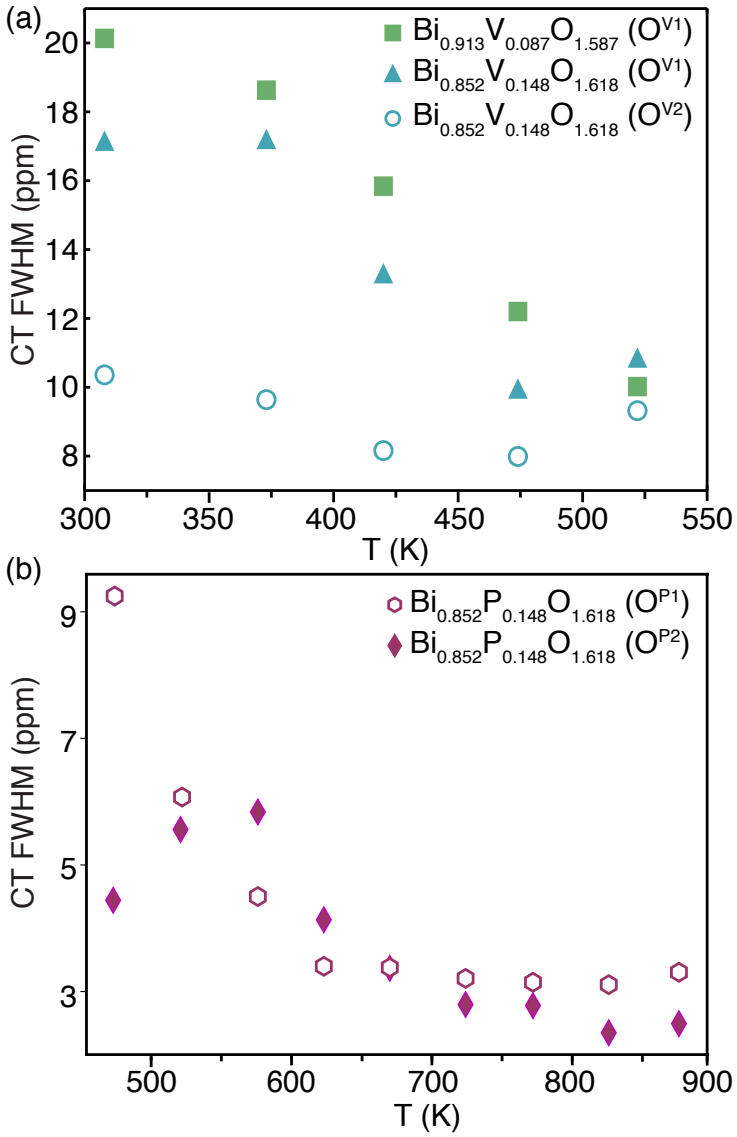

Figure 5: ^{17}O MAS NMR CT full width at half maximum (FWHM) linewidths of the O^V and O^P environments in the three phases as a function of temperature. (a) In both V-substituted samples, one resonance at ∼620 ppm (O^{V1}) narrows with increasing temperature, indicative of increasing local tetrahedral motion, until a minimum linewidth is attained; further motional increases lead to a regime in which CT linewidth is insensitive to motion. For the $Bi_{0.852}V_{0.148}O_{1.648}$ sample, a second resonance at ∼630 ppm (O^{V2}) is observed with a relatively temperature-invariant CT linewidth, indicating the presence of VO_4 tetrahedra that do not undergo motion on the spectral timescale. (b) Two distinct O^P resonances at ∼135 ppm (O^{P1}) and ∼145 ppm (O^{P2}) are resolved for $Bi_{0.852}P_{0.148}O_{1.648}$ at temperatures >473 K. The linewidth of both resonances narrows with increasing temperature (albeit with an initial broadening for the resonance at 145 ppm), reaching a minimum value at ∼650 K.

thus provide insights into the underlying oxide-ion motional mechanisms that distinguish the V-substituted samples. Both V-substituted compounds share a common O^{V1} environment centred at $\sim$620 ppm at room temperature, which narrows as a function of increasing temperature, reaching a minimum CT linewidth between 473 and 523 K (Figure 5a). This environment therefore undergoes thermally-activated ionic motion with a motional rate eventually exceeding the range to which the CT linewidth is sensitive, with no further narrowing above 523 K until coalescence occurs (see SI). By contrast, the linewidth of the second, higher-frequency O^{V2} peak (at $\sim$630 ppm at room temperature), which is only seen for $Bi_{0.852}V_{0.148}O_{1.648}$, retains a relatively constant linewidth over the same temperature range. The observation of two distinct O^{V} environments implies that full local isotropic O exchange is not occurring at these temperatures. Similar narrowing behaviour is seen in the CT linewidth for the O^{Bi} environment in both V-substituted samples (see SI), also suggesting ionic motion on the Bi–O sublattice. However, the extent of narrowing is greater for $Bi_{0.913}V_{0.087}O_{1.587}$ than for $Bi_{0.852}V_{0.148}O_{1.648}$, again implying faster motion, a smaller distribution of local O^{Bi} chemical environments, or both.

For the $Bi_{0.852}P_{0.148}O_{1.648}$ sample, the ^{17}O resonances corresponding to the O^{P} environment(s) also display different behaviours across distinct temperature ranges. From room temperature to $\sim$373 K, what appears to be a single resonance first broadens with increasing temperature, before narrowing at a slightly higher chemical shift (see SI). This unusual behaviour could be due to coalescence of multiple O^{P} resonances (some of which are hidden under the O^{Bi} resonance at room temperature) due to local O rotations within isolated PO_4 units. Above 523 K, another feature appears at 145 ppm, indicating the presence of an additional O^{P} chemical environment (Figure 3 and Figure S3). Both features undergo linewidth narrowing with increasing temperature (see Figure 5b and the SI) and move to higher chemical shifts. As described later (see Discussion), the observed resonances correspond to subtly different local O^{P} environments that persist at high temperatures, a phenomenon which may also occur for the O^{V} environments in $Bi_{0.852}V_{0.148}O_{1.648}$ but cannot be directly observed because of coalescence with the O^{Bi} feature.

^{51}V NMR

The room-temperature ^{51}V MAS NMR spectra for the more highly V-substituted monoclinic sample, $Bi_{0.852}V_{0.148}O_{1.648}$, shown in Figure 6 (right), reveal three major distinct features with isotropic shifts at −487, −493 and −508 ppm, with broad spinning sideband manifolds arising from the corresponding satellite transitions or STs (^{51}V is a quadrupolar nucleus with I = 7/2). Room-temperature ^{51}V NMR spectra taken at higher spinning speed (10 kHz) more easily allow the three distinct environments to be observed (shown in the SI), but unfortunately we could not acquire VT-NMR spectra at very high temperatures at this relatively fast MAS rate. The relatively small difference in chemical shift of these V environments is most likely due to small differences in the local structure surrounding the VO_4 tetrahedra. The resonances lie within the known shift range for 4- and 5-coordinate vanadium sites,[26] with the higher-frequency resonance at −487 ppm likely to be more 5-coordinate in nature, i.e., to experience 5-coordinate bonding environments a greater percentage of the time, as suggested by previous AIMD simulations also showing average V coordination numbers up to 4.3.[23,24]

With increasing temperature, the ^{51}V spinning sideband manifolds of $Bi_{0.852}V_{0.148}O_{1.648}$ first broaden, before reappearing and narrowing up to 823 K. We assign these characteristic changes to increasing rates of ionic motion on the order of the MAS rate (*i.e.*, ∼4 kHz), as seen in similar studies.[27,45–47] In particular, the relevant time scale for this process is influenced by the strengths of anisotropic spin interactions that give rise to the sidebands, primarily quadrupolar coupling for ^{51}V but to a lesser extent chemical shift anisotropy (CSA).[27] The three features remain distinct, with a gradual change to higher frequencies of −456, −472 and −505 ppm, at 673 K. The large change in the shift of the first site in particular is consistent with an increase in coordination number consistent with the formation of VO_5,[48] while the latter two sites remain closer to 4-coordinate. The fact that all three signals persist at high temperature implies their local structural environments remain distinct, even with very fast rates of nearby O^{2-} ion exchange.

The corresponding VT spectra of the lower V-substituted, pseudo-cubic phase $Bi_{0.913}V_{0.087}O_{1.587}$, however, show evidence for only one type of V environment centred at −478 ppm (Figure 6, left)

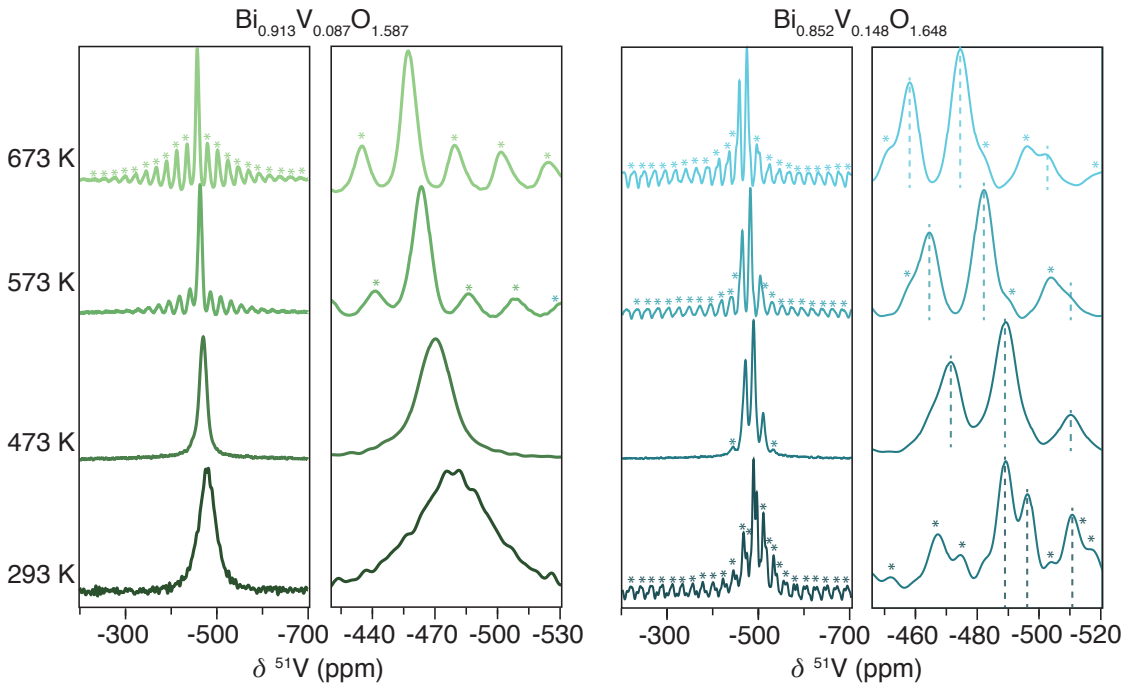

Figure 6: Variable-temperature ^{51}V MAS NMR spectra of $Bi_{0.913}V_{0.087}O_{1.587}$ and $Bi_{0.852}V_{0.148}O_{1.648}$ obtained at 16.4 T at a spinning rate of 4 kHz, with a recycle delay of 0.5 s. At room temperature, the isotropic resonance in the ^{51}V NMR spectrum of $Bi_{0.913}V_{0.087}O_{1.587}$ is already broadened, indicating significantly fast motion involving the VO_4 environment with respect to the spinning frequency, whereas the corresponding spectrum of $Bi_{0.852}V_{0.148}O_{1.648}$ indicates a relatively slower motional rate. Asterisks denote spinning sidebands (for $Bi_{0.913}V_{0.087}O_{1.587}$ only shown at highest temperature for clarity). For $Bi_{0.852}V_{0.148}O_{1.648}$, dashed lines mark the three isotropic resonances; some spinning sidebands appear as shoulders next to, or nearly on top of, the isotropic resonances.

with a much broader CT linewidth at room temperature and no observed ST spinning sideband intensity, consistent with a distribution of similar VO_4 polyhedra. Upon heating, the CT linewidth narrows markedly, accompanied by the appearance and then linewidth narrowing of spinning sidebands; interestingly, this corresponds to the higher-temperature behaviour of the V sites in the highly V-substituted sample ($Bi_{0.852}V_{0.148}O_{1.648}$). As with $Bi_{0.852}V_{0.148}O_{1.648}$, a similar shift change to lower frequency (−458 ppm) occurs, corresponding to an average increase in V coordination. We can conclude that the motion probed by the single V environment, even at room temperature, is already of a similar rate to the MAS spinning frequency (4 kHz) and therefore much faster than that experienced by the equivalent sites in $Bi_{0.852}V_{0.148}O_{1.648}$. Additionally, there is no evidence of additional V environments as in the lower V-substituted $Bi_{0.913}V_{0.087}O_{1.587}$. These results from ^{51}V NMR are in good agreement with the ^{17}O NMR data, in which at moderate temperatures up to coalescence, only one average feature in the V–O region is observed for $Bi_{0.913}V_{0.087}O_{1.587}$, but two such peaks are present for $Bi_{0.852}V_{0.148}O_{1.648}$.

^{31}P NMR

The room temperature ^{31}P MAS NMR spectra of $Bi_{0.852}P_{0.148}O_{1.648}$ comprise a single broad resonance that narrows with increasing temperature (Figure 7), allowing us to distinguish four different local environments. We assign these linewidth changes to the influence of nearby oxygen motion that enters the fast motional regime at high temperature and thus no longer broadens the ^{31}P resonances, a result that concurs with the narrowing linewidths seen in the corresponding ^{17}O spectra. At high temperatures, the four distinct ^{31}P resonances reflect small changes in the number and arrangement of nearby Bi and P atoms, in good agreement with the four reported crystallographic P sites in the monoclinic $Bi_{0.852}P_{0.148}O_{1.648}$ structure.[25] This same resolution is not achieved in the ^{51}V spectra, which is ascribed to some second-order quadrupolar line broadening of ^{51}V (I = 7/2) that persists even at high temperatures, as well as most likely increased disorder of the VO_x polyhedra as compared to PO_4.

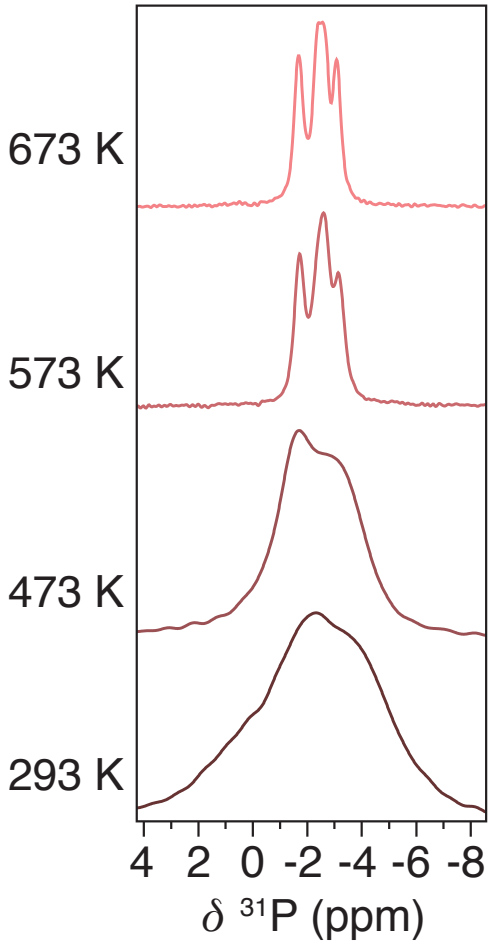

Figure 7: Variable-temperature ^{31}P MAS NMR spectra of $Bi_{0.852}P_{0.148}O_{1.648}$ obtained at 16.4 T at a spinning rate of 4 kHz, with a recycle delay of 30 s. At room temperature, the ^{31}P NMR spectrum shows a single highly broadened feature similar to the ^{51}V NMR spectra of $Bi_{0.913}V_{0.087}O_{1.587}$. A narrowing isotropic linewidth is seen with increasing temperature that reveals four distinct ^{31}P resonances.

^{17}O T_1 measurements

Measurement of the spin-lattice (T_1) relaxation times as a function of temperature can be used to gain insight into ionic motion correlation rates on the order of the Larmor frequency ($\sim 10^8$ Hz), a motional regime well above that accessible through CT linewidth measurements, which are only sensitive to motion on the order of the MAS rate ($\sim 10^4 - 10^5$ Hz). (We note that T_1 measurements may also probe a range of motional rates several orders of magnitude above and below the Larmor frequency, depending on the specific relaxation mechanism(s) and the temperature of the system.) By measuring the ^{17}O T_1 values for both the O^{Bi} and O^{V} sites as a function of temperature, the relative contributions to ionic motion in these materials can be determined. Results from ^{17}O T_1 measurements for $Bi_{0.913}V_{0.087}O_{1.587}$, $Bi_{0.852}V_{0.148}O_{1.648}$ and $Bi_{0.852}P_{0.148}O_{1.648}$ are shown in Figure 8.

For all three materials, the ^{17}O T_1 of the O^{Bi} environment decreases with increased temperature, suggestive of changes in ionic motion within the Bi–O sublattice on the MHz timescale. The motion involving the Bi–O sublattice as probed by the T_1 relaxation measurements is ascribed to the local movement of oxygen vacancies, which have previously been measured with ^{17}O NMR relaxometry in other oxide-ion conductors, *e.g.*, Y-doped ceria[49] and Bi_2WO_6.[38] The relevant motions in these systems contributing to temperature-dependent changes in the T_1 values are typically considered to comprise short-range displacements such as nearest neighbour and/or nearby vacancy jumps,[50] which may be distinct from motions influencing bulk ionic conductivity.

On the other hand, the T_1 values for the O^{V} environments in both V-substituted materials have a weaker dependence on temperature. While the earlier linewidth analysis of the O^{V} environment clearly probes increasing local VO_4 rotational or librational motion, the lack of any change to the T_1 relaxation rates would suggest that this motion is not in the sensitive regime centred about the Larmor frequency (i.e., $\sim 10^6$ to $\sim 10^{10}$ Hz). We note that the T_1 values for the O^{V} site are surprisingly short; the previous ^{17}O NMR study of $Bi_{26}Mo_{10}O_{69}$ by Holmes *et al.*[27] also found comparably short T_1 times ($\sim$10 ms at and above room temperature) for MoO_4 tetrahedral units. At higher temperatures the T_1 values for the O^{Bi} and O^{V} environments appear to converge,

consistent with earlier observed coalescence of these two sites and the accompanying averaging of their apparent ^{17}O quadrupolar parameters. This supports the inference that quadrupolar relaxation mechanism leads to the observed changes in T_1.

The O^P environment in $Bi_{0.852}P_{0.148}O_{1.648}$ appears to have a short, temperature-invariant T_1 value of $\sim$1 ms, as shown in the SI, although signal from this site could not be deconvoluted at several temperatures in the ^{17}O relaxation measurements due to overlap with the O^{Bi} resonance.

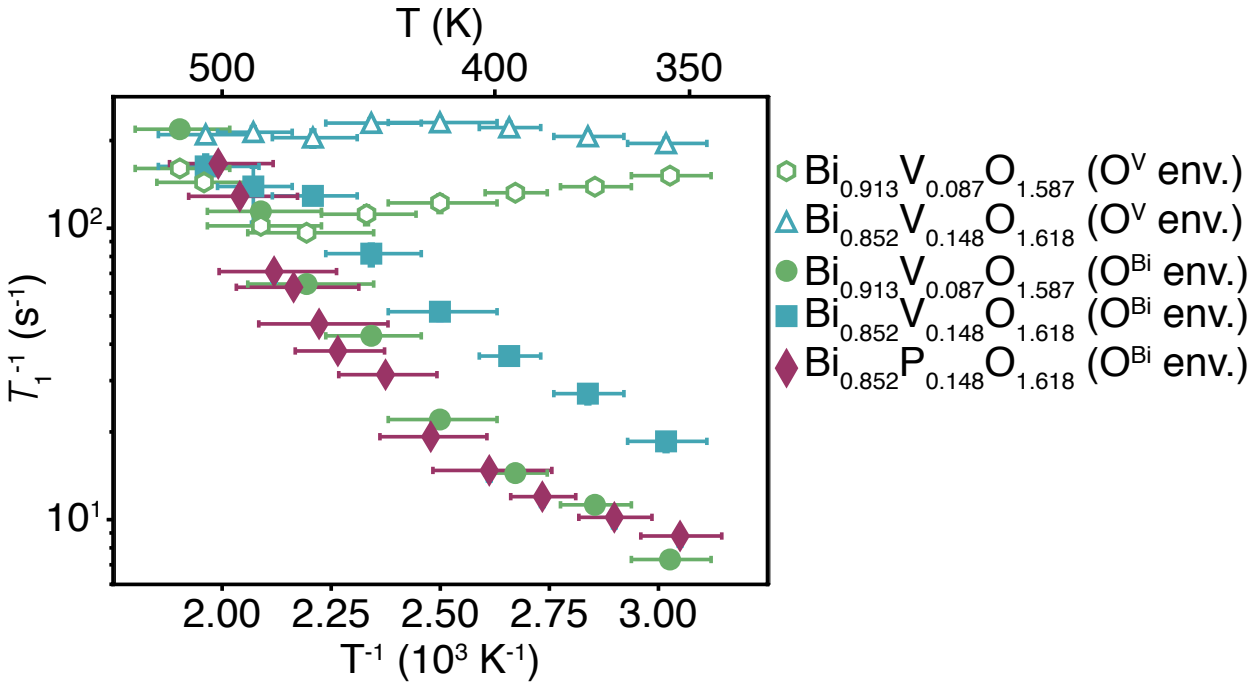

Figure 8: Inverse ^{17}O relaxation rates (T_1^{-1}) as a function of inverse temperature for $Bi_{0.913}V_{0.087}O_{1.587}$, $Bi_{0.852}V_{0.148}O_{1.648}$ and $Bi_{0.852}P_{0.148}O_{1.648}$, for both the O^{Bi} and O^V environments. In the case of $Bi_{0.852}V_{0.148}O_{1.648}$, the two distinct O^{V1} and O^{V2} environments (at $\sim$620 and $\sim$630 ppm) have similar T_1^{-1} values and the features have been analysed together. In the case of $Bi_{0.852}P_{0.148}O_{1.648}$, T_1 values for the O^P environment were consistently too short to reliably measure (< 1 ms) and/or the O^P features were not resolved at certain temperatures due to overlap with the O^{Bi} resonance.

Activation energies

If it is assumed that the temperature dependence of the spin-lattice (T_1) relaxation of the O^{Bi} site(s) is driven by transient, motion-induced changes in the apparent ^{17}O quadrupolar coupling,

activation energies for oxide ion and/or vacancy mobility can be extracted. In this analysis, inverse correlation times τ_c^{-1} are first calculated, which can be derived from fits to the T_1 data using the following equation:[51,52]

$$\frac{1}{T_1} = \frac{2\pi^2}{25} \cdot C_Q^2 \cdot \left(1 + \frac{\eta_Q^2}{3}\right) \cdot \left[\frac{\tau_c}{1+\omega_0^2\tau_c^2} + \frac{4\tau_c}{1+4\omega_0^2\tau_c^2}\right], \quad (1)$$

where ω_0 is the Larmor frequency of ^{17}O (67.83 MHz at 11.7 T), and values of the proportionality constant $C_Q^2 \cdot \left(1 + \frac{\eta_Q^2}{3}\right)$, which depend on the estimated quadrupole coupling constant C_Q and quadrupolar asymmetry parameter η_Q of the O^{Bi} environments, have been obtained by acquiring room-temperature spectra at multiple magnetic fields and determining the field dependence of the second-order quadrupolar shift (further details in Supplementary Information).

If we then take the τ_c^{-1} values to be equal to the average jump rates τ^{-1} for the relevant motional processes, we can fit the linear parts of each curve to extract an activation energy E_A and pre-exponential factor τ_i^{-1} for the ionic motion, using the Arrhenius relationship:[52]

$$\tau^{-1} = \tau_i^{-1} \cdot \exp\left(-\frac{E_A}{k_B T}\right) \quad (2)$$

Given that exchange at higher temperatures leads to an apparent average C_Q value between the O^V and O^{Bi} sites, we have restricted this fitting to temperatures ≤ 400 K to obtain an accurate value for motion within the Bi–O sublattice solely. The results of this fitting are shown in Figure 9 and Table 1. All samples have similar E_A values within error, consistent with a common oxide ion motion present within the Bi–O sublattice.

A similar Arrhenius relationship can also be applied to the temperature-dependent ^{17}O CT linewidth(s) for the O^V and O^P environments plotted in Figure 5, under the assumption that this variation is related to changes in the rate of oxide-ion motion. In this analysis, the logarithm of the inverse CT linewidth is plotted against inverse temperature, which gives a linear relationship when the relevant motional rate is on the order of the MAS rate, *i.e.*, typically when the rate is between 100 Hz and 10 kHz.[45–47,53] The results of the linewidth fitting are shown in Figure 10 and Table 1.

In contrast to that of the O^V and O^P environments, the ^{17}O CT linewidths of the O^{Bi} features display more complicated behaviour with new environments appearing and disappearing at different temperatures; therefore, E_A values could not be reliably derived in this way (see SI).

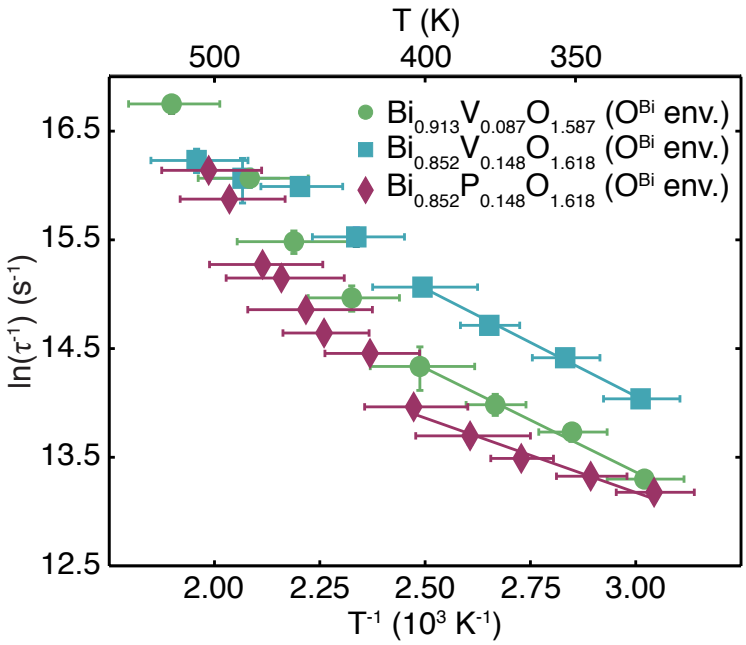

Figure 9: Arrhenius fitting of the inverse correlation times τ^{-1} which have been extracted from the inverse ^{17}O relaxation rates T_1^{-1} of the O^{Bi} environments; the E_A derived from the low temperature region corresponds to local motion within the Bi–O sublattice.

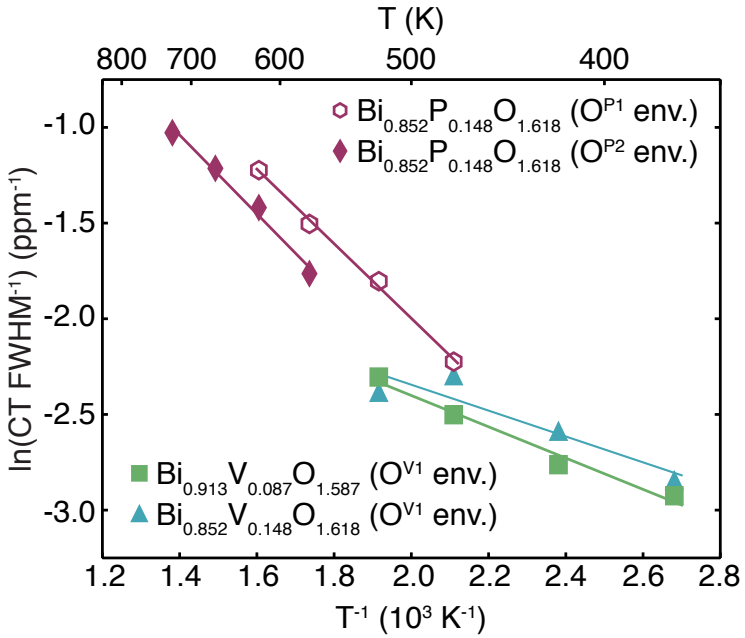

Figure 10: Arrhenius fitting of inverse ^{17}O CT linewidths of the O^{V} and O^{P} environments. The O^{P1} and O^{P2} environments correspond to the peaks at ∼135 ppm and ∼145 ppm, respectively, and the O^{V1} environment corresponds to the peak at ∼620 ppm (the other O^{V2} site has a temperature-invariant linewidth). The E_A derived in this way corresponds to oxide-ion motion within the VO_4 and PO_4 polyhedral units, such as rotations or librations, on the spectral timescale (typically on the order of ∼1 kHz).

Table 1: Activation energies E_A of oxide ion motion for the materials studied, determined from ^{17}O relaxation (T_1) measurements and analysis of the ^{17}O CT linewidths. Activation energies derived from the ^{17}O T_1 values for the O^{P} environment(s) in $Bi_{0.852}P_{0.148}O_{1.648}$ are not reported, as the T_1 values were consistently too small to reliably measure (< 1 ms), or the spectral features were not resolved at certain temperatures due to overlap with the O^{Bi} resonance.

Sample	Method	Environment	E_A (eV)
$Bi_{0.913}V_{0.087}O_{1.587}$	T_1	O^{Bi}	0.16 ± 0.02
$Bi_{0.852}V_{0.148}O_{1.648}$	T_1	O^{Bi}	0.16 ± 0.02
$Bi_{0.852}P_{0.148}O_{1.648}$	T_1	O^{Bi}	0.11 ± 0.02
$Bi_{0.913}V_{0.087}O_{1.587}$	CT linewidth (620 ppm)	O^{V1}	0.07 ± 0.02
$Bi_{0.852}V_{0.148}O_{1.648}$	CT linewidth (620 ppm)	O^{V1}	0.06 ± 0.02
$Bi_{0.852}P_{0.148}O_{1.648}$	CT linewidth (135 ppm)	O^{P1}	0.04 ± 0.02
$Bi_{0.852}P_{0.148}O_{1.648}$	CT linewidth (145 ppm)	O^{P2}	0.04 ± 0.02

Discussion

The previously published structural and AIMD studies of these systems[23,24] suggested that long-range, isotropic oxide-ion motion in $Bi_{0.852}V_{0.148}O_{1.648}$ and $Bi_{0.913}V_{0.087}O_{1.587}$ takes place through exchange between the Bi–O and VO_4 sublattices, facilitated by the variable coordination number of V. The ^{17}O VT MAS NMR spectra clearly support this mechanism, as the coalesced resonances observed at high temperatures are directly indicative of a motionally averaged O environment rapidly sampling both O^{Bi} and O^{V} sites, albeit occurring at a slower rate than the local motional processes within the Bi–O sublattice. Moreover, the coalesced ^{17}O shift lying closer to that of the position of the O^{V} resonance than would be expected purely from stoichiometry implies the presence of over-coordinated V sites, with the average O environment residing more frequently near V. These results agree with the ^{51}V resonances measured between −450 and −510 ppm (Figure 6), which are consistent with both 4- and 5-coordinate vanadium environments observed previously,[48,54,55] as well as a change towards more highly-coordinated V sites (higher frequency ^{51}V shifts) at higher temperatures; we do however note that the isotropic ^{51}V shifts are difficult to fully resolve at the slow spinning speeds used in the VT-NMR experiments.

For $Bi_{0.852}P_{0.148}O_{1.648}$, the E_A values found for motion within the PO_4 units agree relatively well with the small activation barriers for tetrahedral rotation previously found using ^{17}O NMR in tetraoxoanion-containing materials,[56] indicating that the relatively straightforward CT linewidth analysis nonetheless leads to reasonable activation energy values. Moreover, the E_A values are identical within error to those obtained for motion involving the VO_4 units in the V-substituted materials, suggesting that similar motional processes operate in both types of dopant sublattices.

This study also provides insight as to the different local oxide-ion conduction mechanisms operating in the different phases. The previously measured differences in bulk ionic conductivity for $Bi_{0.913}V_{0.087}O_{1.587}$ and $Bi_{0.852}V_{0.148}O_{1.648}$ ($\sigma \approx 10^{-2}$ and 10^{-3} S cm^{-1} at 673 K, respectively) now become apparent in terms of variations in the O^{V} environments present in these materials. For the more highly V-substituted, monoclinic $Bi_{0.852}V_{0.148}O_{1.648}$, two distinct types of O^{V} environments are observed (O^{V1} and O^{V2}), with different rates of associated O motion as revealed

by the differences in the temperature dependence of their ^{17}O CT linewidths. By comparison, only a single O^{V1} environment is resolved for $Bi_{0.913}V_{0.087}O_{1.587}$. We note that the O^{V1} site in $Bi_{0.852}V_{0.148}O_{1.648}$ and $Bi_{0.913}V_{0.087}O_{1.587}$ has a very similar chemical shift (∼620 ppm) and temperature-dependent linewidth behaviour in both samples, which we ascribe to O in a more highly-coordinated local VO_4 environment with a faster rate of local motion and/or sublattice exchange. The appearance of the second O^{V2} resonance in $Bi_{0.852}V_{0.148}O_{1.648}$ with a temperature-invariant ^{17}O CT linewidth is indicative of O sites that do not participate to the same degree in exchange and instead may hinder long-range oxygen motion. Structurally, the presence of these additional O^{V2} environment(s) is a consequence of higher V-doping and is consistent with shorter distances between neighbouring VO_4 tetrahedra.[20] Interestingly, two O^{P} sites also appear in the ^{17}O spectra of $Bi_{0.852}P_{0.148}O_{1.648}$ (O^{P1} and O^{P2}), and in both the P- and V-substituted samples we observe a ∼1:3 intensity ratio of the two sites at higher temperatures (see Figure 4 and SI). We note the $Bi_{0.852}V_{0.148}O_{1.648}$ and $Bi_{0.852}P_{0.148}O_{1.648}$ phases are structurally analogous, and possess four crystallographically distinct P/V sites;[25] in the reported crystal structures, one of the P/V sites appears to possess different local tetrahedral distortions, which may give rise to the distinct oxygen environments with the ∼1:3 intensity ratio we observe.

The ^{17}O VT-NMR spectra of $Bi_{0.852}P_{0.148}O_{1.648}$ (Figure 3) indicate conduction processes that differ from the sublattice exchange evident from the two-site coalescence observed for the V-substituted samples. Focussing on the O^{Bi} region of the spectra, three distinct regimes are active at different temperatures. From room temperature to 473 K, only one broad O^{Bi} resonance is observed, consistent with slow ionic motion and/or a large chemical shift distribution that prevents the resolution of individual sites. From 523–673 K two distinct environments at ∼220 and ∼200 ppm are resolved, which are tentatively ascribed to O near, and not near, an oxide ion vacancy in the Bi–O sublattice; this assignment is consistent with the oxygen vacancies observed in this phase previously.[25] (We note a two-peak fit is justified as second-order quadrupolar coupling lineshapes are not expected, with further details given in the SI.) At these temperatures, the higher-frequency resonance at ∼220 ppm displays a narrowing linewidth with increasing temperature. We attribute

this behaviour to the vacancy-adjacent oxygen atoms undergoing hopping into vacancy sites. By contrast, the isolated oxygens in fully occupied regions of the lattice are immobile, and therefore the corresponding spectral feature (at ∼200 ppm) exhibits an invariant linewidth with increasing temperature. (Two O^{Bi} resonances at ∼220 ppm and ∼200 ppm are also observed in the ^{17}O spectra of both V-substituted samples, especially in the spectra collected at 573 K, showing that O sites adjacent to vacancies can be distinguished in all the studied phases.)

Finally, at temperatures >723 K, the two O^{Bi} environments in the P-substituted material coalesce to a single peak due to sufficiently rapid oxide-ion motion within the entire Bi–O sublattice, *i.e.*, on the NMR timescale, no O sites are isolated from vacancies. Over the same temperature range, both the ^{17}O and ^{31}P NMR spectra reveal an increasing number of different O^{P} environments that can be resolved due to motional narrowing; however, this motion must be restricted to localised tetrahedral rotations because coalescence between the Bi–O and PO_4 sublattices is not observed. In contrast, the same behaviour cannot be observed in ^{17}O NMR spectra of the V-substituted samples due to the coalescence of the O^{Bi} and O^{V} resonances; however, the ^{51}V NMR spectra of $Bi_{0.852}V_{0.148}O_{1.648}$ still indicate the presence of V sites with differing coordination numbers even at high temperature.

The variable coordination of the dopant ion plays a crucial role in understanding the differing ionic conductivities of these fluorite-type materials. Experimentally, the $Bi_{0.852}P_{0.148}O_{1.648}$ exhibits the lowest conductivity, followed by $Bi_{0.852}V_{0.148}O_{1.648}$ and $Bi_{0.913}V_{0.087}O_{1.587}$.[23,24,28] Although dopants clearly aid in stabilising the cubic δ-Bi_2O_3 structure, they also tend to disrupt three-dimensional isotropic conduction within the Bi–O sublattice. However, to a limited degree cooperative exchange between the dopant and Bi–O sublattices can offset this effect. The difference in the conductivity of pseudo-cubic $Bi_{0.913}V_{0.087}O_{1.587}$ and monoclinic $Bi_{0.852}V_{0.148}O_{1.648}$ highlights this first point, with the maintenance of the long-range 3D isotropic structure in the former case contributing to its exceptional ionic conduction. In the case of $Bi_{0.852}P_{0.148}O_{1.648}$, although increasing rates of oxide-ion motion clearly do occur within the Bi–O sublattice as we have shown, the inability of phosphorus to adopt variable O coordination hinders significant sub-

lattice exchange and leads to overall lower bulk conductivity. Similar observations have been made regarding the $Bi_{28}Re_2O_{49}$[57] and $Bi_{1-x}Nb_xO_{1.5+x}$[58] phases, which utilise dopant atoms that adopt variable O coordination, but also undergo doping-induced symmetry lowering of the crystal structure from cubic to tetragonal; this in turn leads to correspondingly lower oxide-ion conductivity than in the vanadate materials.

Seen in the context of previous studies on oxygen ion conductors, and Bi-based materials in particular, our results further consolidate the state of mechanistic understanding of the conduction processes, while also adding local-level insights regarding structure and dynamics. Firstly, conduction in the V-substituted materials appears to operate in a similar fashion to $Bi_{26}Mo_{10}O_{69}$,[27] with rapid localised rotation measured for dopant polyhedra at low temperatures preceding the onset of long-range, isotropic conduction *via* cooperative exchange with the Bi-containing sublattice at higher temperatures. However, in the $Bi_{26}Mo_{10}O_{69}$ system the onset of sublattice exchange appears correlated with and possibly driven by a monoclinic-triclinic phase transition at 583 K, in contrast to the temperature-invariant structures of the vanadates and phosphates studied here. Also, the previous work on the molybdates as well as other solid-state ^{17}O NMR results indicating rapid polyhedral rotation at low temperatures (e.g., E_A = 0.07 eV in $KMnO_4$[56]) give us confidence that the very small activation energies for VO_4 and PO_4 rotation do indeed represent local rotational or librational motion. Finally, as discussed in the prior study of Kim and Grey on V- and Ti-substituted Bi_2O_3 materials,[26] distorted polyhedra are critical in facilitating ionic mobility. In that work, of the three local V environments (symmetric tetrahedral, symmetric pentahedral and distorted tetrahedral) present in α-$Bi_4V_2O_{11}$ and observed by ^{51}V NMR, the most distorted environment was associated with the highest oxide-ion mobility, as probed by variable-temperature $^{51}V\{^{17}O\}$ TRAPDOR NMR experiments. This mirrors our results which suggest that distorted and overcoordinated VO_4 polyhedra contribute to higher oxygen conductivity for $Bi_{0.913}V_{0.087}O_{1.587}$, while the presence of additional, more symmetric ^{51}V environments in $Bi_{0.852}V_{0.148}O_{1.648}$ are responsible for the slightly lower oxygen conductivity of this phase.

Conclusions

In this work, a multinuclear VT MAS NMR approach has been applied to elucidate the influence of V and P substitution on the oxide-ion conductivity of promising stabilised bismuth oxide (δ-Bi_2O_3) phases. We have shown that variable-temperature solid-state NMR is particularly well-suited to understanding connections between local structural features and ionic mobility, and can quantify the evolution of ion dynamics with temperature.

Initially, room temperature ^{17}O MAS NMR measurements have been performed to characterise the local O environments present in each material; we are able to distinguish between bismuth oxide-like (O^{Bi}) environments and other sites corresponding to VO_4 (O^V) and PO_4 (O^P) polyhedral units. Next, upon heating the V-substituted samples, the resonances arising from these chemically distinct sublattices first sharpen, then disappear, and finally reappear as a single coalesced (averaged) peak at high temperature, conclusively showing oxide-ion exchange between the two sublattices. In contrast, ^{17}O NMR spectra of the phosphate phase do not evidence two-site coalescence within the studied temperature range (up to 873 K); we conclude this material exhibits a different and less effective oxide-ion conduction mechanism, as supported by lower values of ionic conductivity measured previously.[23,24,28]

Arrhenius-based analyses of both the ^{17}O T_1 relaxation rates and central transition (CT) linewidth data allow us to determine activation energies for thermally-activated motional processes within the two distinct sublattices (Bi–O and VO_4/PO_4); the much lower activation energy for local VO_4 rotations or librations as compared to those of PO_4 helps to explain the differences in bulk conductivity between the materials. Furthermore, two different O^V environments are observed for the higher V-substituted phase $Bi_{0.852}V_{0.148}O_{1.648}$. We argue that with increased V doping, symmetry lowering from pseudo-cubic to monoclinic leads to two different types of local VO_4 environments with differing rates of local ionic motion, which in turn disrupts the three-dimensional oxide-ion conduction network. These findings highlight the crucial interplay between dopant concentration and the long-range ionic conduction pathways, and also point out the influence of the coordination flexibility of the dopant. These two factors (dopant concentration and coordination) directly

affect the available oxide-ion mobility mechanisms in Bi_2O_3-based materials and thus determine the overall functional performance.

In summary, this study highlights the potential for multinuclear variable-temperature solid-state NMR, with its specificity for different nuclei as well as sensitivity to local dynamics, to provide unique insights into the underlying mechanisms driving bulk ionic conduction in superionic conductors. In turn, these mechanisms suggest design rules that can be utilised in future work to optimise the next generation of ionic conducting materials with the ultimate goal of rational materials design.

Acknowledgement

M.T.D. is supported by a Junior Research Fellowship from Clare College, Cambridge, and a STFC Early Career Award. D.M.H. acknowledges funding from the Cambridge Commonwealth Trusts, and is grateful for support from NECCES, an Energy Frontier Research Center funded by the U.S. Department of Energy, Office of Science, Office of Basic Energy Sciences under Award No. DE-SC0012583. I.R.E. acknowledges the Royal Society and the Leverhulme Trust for the award of a Senior Research Fellowship.

Supporting Information

XRD characterisation, complete VT-NMR datasets, details of ^{17}O quadrupolar parameter fitting, further ^{17}O NMR saturation recovery and CT data.

Data

All supporting data for this work can be found on https://www.repository.cam.ac.uk.

References

(1) Sunarso, J.; Hashim, S. S.; Zhu, N.; Zhou, W. Perovskite Oxides Applications in High Temperature Oxygen Separation, Solid Oxide Fuel Cell and Membrane Reactor: A Review. *Progress in Energy and Combustion Science* **2017**, *61*, 57 – 77.

(2) Mahato, N.; Banerjee, A.; Gupta, A.; Omar, S.; Balani, K. Progress in Material Selection for Solid Oxide Fuel Cell Technology: A Review. *Prog. Mater. Sci.* **2015**, *72*, 141–337.

(3) Aguadero, A.; Fawcett, L.; Taub, S.; Woolley, R.; Wu, K.-T.; Xu, N.; Kilner, J. A.; Skinner, S. J. Materials Development for Intermediate-Temperature Solid Oxide Electrochemical Devices. *J. Mater. Sci.* **2012**, *47*, 3925–3948.

(4) Steele, B. C. H.; Heinzel, A. Materials for Fuel-Cell Technologies. *Nature* **2001**, *414*, 345–352.

(5) Gattow, G.; Schröder, H. Über Wismutoxide. III. Die Kristallstruktur Der Hochtemperaturmodifikation von Wismut(III)-Oxid (δ-Bi2O3). *Z. anorg. allg. Chem.* **1962**, *318*, 176–189.

(6) Takahashi, T.; Iwahara, H.; Nagai, Y. High Oxide Ion Conduction in Sintered Bi2O3 Containing SrO, CaO or La2O3. *J Appl Electrochem* **1972**, *2*, 97–104.

(7) Wachsman, E. D. Effect of Oxygen Sublattice Order on Conductivity in Highly Defective Fluorite Oxides. *Journal of the European Ceramic Society* **2004**, *24*, 1281–1285.

(8) Verkerk, M. J.; Burggraaf, A. J. High Oxygen Ion Conduction in Sintered Oxides of the Bi2 O 3 - Dy2 O 3 System. *J. Electrochem. Soc.* **1981**, *128*, 75–82.

(9) Punn, R.; Feteira, A. M.; Sinclair, D. C.; Greaves, C. Enhanced Oxide Ion Conductivity in Stabilized δ-Bi2O3. *J. Am. Chem. Soc.* **2006**, *128*, 15386–15387.

(10) Jiang, N.; Wachsman, E. D. Structural Stability and Conductivity of Phase-Stabilized Cubic Bismuth Oxides. *Journal of the American Ceramic Society* **1999**, *82*, 3057–3064.

(11) Iwahara, H.; Esaka, T.; Sato, T.; Takahashi, T. Formation of High Oxide Ion Conductive Phases in the Sintered Oxides of the System Bi2O3-Ln2O3 (Ln = La-Yb). *Journal of Solid State Chemistry* **1981**, *39*, 173–180.

(12) Drache, M.; Roussel, P.; Wignacourt, J.-P. Structures and Oxide Mobility in Bi-Ln-O Materials: Heritage of Bi2O3. *Chem. Rev.* **2007**, *107*, 80–96.

(13) Đorđević, T.; Karanović, L. A New Anion-Deficient Fluorite-Related Superstructure of Bi28V8O62. *Journal of Solid State Chemistry* **2014**, *220*, 259–269.

(14) Watanabe, A.; Kitami, Y. An Outline of the Structure of Oxide-Ion Conductors Bi23V4-4xP4xO44.5 ($0 \leq x \leq 1$). *Solid State Ionics* **1998**, *113*, 601–606.

(15) Wignacourt, J. P.; Drache, M.; Confiant, P.; Boivin, J. C. Nouvelles phases du système Bi2O3-BiPO4 I. Description du diagramme de phases. *J. Chim. Phys.* **1991**, *88*, 1933–1938.

(16) Wignacourt, J. P.; Drache, M.; Conflant, P. A New Oxide Ion Conductor Family: Bi7(P1-yVy)O13. *Journal of Solid State Chemistry* **1993**, *105*, 44–48.

(17) Takahashi, T.; Iwahara, H.; Esaka, T. High Oxide Ion Conduction in Sintered Oxide of the System Bi2 O 3 - M 2 O 5. *J. Electrochem. Soc.* **1977**, *124*, 1563–1569.

(18) Sammes, N. M.; Tompsett, G. A.; Näfe, H.; Aldinger, F. Bismuth Based Oxide Electrolytes—Structure and Ionic Conductivity. *Journal of the European Ceramic Society* **1999**, *19*, 1801–1826.

(19) Zhou, W. Defect Fluorite-Related Superstructures in the Bi2O3-V2O5 System. *Journal of Solid State Chemistry* **1988**, *76*, 290–300.

(20) Zhou, W. The Type II Superstructural Family in the Bi2O3-V2O5 System. *Journal of Solid State Chemistry* **1990**, *87*, 44–54.

(21) Pang, G.; Feng, S.; Tang, Y.; Tan, C.; Xu, R. Hydrothermal Synthesis, Characterization, and Ionic Conductivity of Vanadium-Stabilized Bi17V3O33 with Fluorite-Related Superlattice Structure. *Chem. Mater.* **1998**, *10*, 2446–2449.

(22) Azad, A. M.; Larose, S.; Akbar, S. A. Bismuth Oxide-Based Solid Electrolytes for Fuel Cells. *J. Mater. Sci.* **1994**, *29*, 4135–4151.

(23) Kuang, X.; Payne, J. L.; Johnson, M. R.; Radosavljevic Evans, I. Remarkably High Oxide Ion Conductivity at Low Temperature in an Ordered Fluorite-Type Superstructure. *Angew. Chem.* **2012**, *51*, 690–694.

(24) Kuang, X.; Payne, J. L.; Farrell, J. D.; Johnson, M. R.; Evans, I. R. Polymorphism and Oxide Ion Migration Pathways in Fluorite-Type Bismuth Vanadate, Bi46V8O89. *Chem. Mater.* **2012**, *24*, 2162–2167.

(25) Darriet, J.; Launay, J. C.; Zúniga, F. J. Crystal Structures of the Ionic Conductors Bi46M8O89 (M=P, V) Related to the Fluorite-Type Structure. *Journal of Solid State Chemistry* **2005**, *178*, 1753–1764.

(26) Kim, N.; Grey, C. P. Probing Oxygen Motion in Disordered Anionic Conductors with 17O and 51V MAS NMR Spectroscopy. *Science* **2002**, *297*, 1317–1320.

(27) Holmes, L.; Peng, L.; Heinmaa, I.; O'Dell, L. A.; Smith, M. E.; Vannier, R.-N.; Grey, C. P. Variable-Temperature 17O NMR Study of Oxygen Motion in the Anionic Conductor Bi26Mo10O69. *Chem. Mater.* **2008**, *20*, 3638–3648.

(28) Watanabe, A. Bi23M4O44.5 (M = P and V): New Oxide-Ion Conductors with Triclinic Structure Based on a Pseudo-Fcc Subcell. *Solid State Ionics* **1997**, *96*, 75–81.

(29) Pawley, G. S. Unit-Cell Refinement from Powder Diffraction Scans. *Journal of Applied Crystallography* **1981**, *14*, 357–361.

(30) Rietveld, H. M. A Profile Refinement Method for Nuclear and Magnetic Structures. *Journal of Applied Crystallography* **1969**, *2*, 65–71.

(31) Coelho, A. A.; Evans, J.; Evans, I.; Kern, A.; Parsons, S. The TOPAS Symbolic Computation System. *Powder Diffraction* **2011**, *26*, S22–S25.

(32) Taulelle, F.; Coutures, J.; Massiot, D.; Rifflet, J. High and Very High Temperature NMR. *Bulletin of Magnetic Resonance* **1989**, *11*, 318–320.

(33) Ernst, H.; Freude, D.; Mildner, T.; Wolf, I. Laser-Supported High-Temperature MAS NMR for Time-Resolved in Situ Studies of Reaction Steps in Heterogeneous Catalysis. *Solid State Nucl. Magn. Reson.* **1996**, *6*, 147–156.

(34) Thurber, K. R.; Tycko, R. Measurement of Sample Temperatures under Magic-Angle Spinning from the Chemical Shift and Spin-Lattice Relaxation Rate of 79Br in KBr Powder. *J. Magn. Reson.* **2009**, *196*, 84–87.

(35) Eckert, H.; Wachs, I. E. Solid-State Vanadium-51 NMR Structural Studies on Supported Vanadium(V) Oxide Catalysts: Vanadium Oxide Surface Layers on Alumina and Titania Supports. *J. Phys. Chem.* **1989**, *93*, 6796–6805.

(36) Hayashi, S.; Hayamizu, K. 51V NMR Chemical Shift and Anisotropy in Solid Metavanadates. *BCSJ* **1990**, *63*, 961–963.

(37) Yang, S.; Park, K. D.; Oldfield, E. Oxygen-17 Labeling of Oxides and Zeolites. *J. Am. Chem. Soc.* **1989**, *111*, 7278–7279.

(38) Kim, N.; Vannier, R.-N.; Grey, C. P. Detecting Different Oxygen-Ion Jump Pathways in Bi2WO6 with 1- and 2-Dimensional 17O MAS NMR Spectroscopy. *Chem. Mater.* **2005**, *17*, 1952–1958.

(39) Colmont, M.; Delevoye, L.; Mentré, O. Evidence of Crystalline/Glassy Intermediates in Bismuth Phosphates. *New Journal of Chemistry* **2009**, *33*, 19–22.

(40) Wagner, G. W. Two-Dimensional Oxygen-17-Vanadium-51 Heteronuclear Shift Correlation NMR Spectroscopy of the 17O-Enriched Inclusion Complex [CH3CN.Cntnd.(V12O324-)]. Relationship of Cross-Peak Intensity to Bond Order. *Inorg. Chem.* **1991**, *30*, 1960–1962.

(41) Kim, G.; Griffin, J. M.; Blanc, F.; Haile, S. M.; Grey, C. P. Characterization of the Dynamics in the Protonic Conductor CsH_2PO_4 by ^{17}O Solid-State NMR Spectroscopy and First-Principles Calculations: Correlating Phosphate and Protonic Motion. *J. Am. Chem. Soc.* **2015**, *137*, 3867–3876.

(42) Kim, G.; Griffin, J. M.; Blanc, F.; Halat, D. M.; Haile, S. M.; Grey, C. P. Revealing Local Dynamics of the Protonic Conductor CsH(PO3H) by Solid-State NMR Spectroscopy and First-Principles Calculations. *J. Phys. Chem. C* **2017**, *121*, 27830–27838.

(43) Stebbins, J. F.; Oglesby, J. V.; Lee, S. K. Oxygen Sites in Silicate Glasses: A New View from Oxygen-17 NMR. *Chemical Geology* **2001**, *174*, 63–75.

(44) Corrie, B. J.; Shin, J. F.; Hull, S.; Knight, K. S.; Vlachou, M. C.; Hanna, J. V.; Slater, P. R. Neutron Diffraction and Multinuclear Solid State NMR Investigation into the Structures of Oxide Ion Conducting La9.6Si6O26.4 and La8Sr2Si6O26, and Their Hydrated Phases. *Dalton Trans.* **2016**, *45*, 121–133.

(45) Dunstan, M. T.; Griffin, J. M.; Blanc, F.; Leskes, M.; Grey, C. P. Ion Dynamics in Li2CO3 Studied by Solid-State NMR and First-Principles Calculations. *J. Phys. Chem. C* **2015**, *119*, 24255–24264.

(46) Hunger, M. Multinuclear Solid-State NMR Studies of Acidic and Non-Acidic Hydroxyl Protons in Zeolites. *Solid State Nuclear Magnetic Resonance* **1996**, *6*, 1–29.

(47) Baba, T.; Inoue, Y.; Shoji, H.; Uematsu, T.; Ono, Y. Temperature-Dependent Lineshape of 1H Magic-Angle Spinning Nuclear Magnetic Resonance Spectra of Acidic Hydroxyl Groups in Zeolites. *Microporous Mater.* **1995**, *3*, 647–655.

(48) Delmaire, F.; Rigole, M.; Zhilinskaya, E. A.; Aboukaïs, A.; Hubaut, R.; Mairesse, G. 51 V Magic Angle Spinning Solid State NMR Studies of Bi4V2O11 in Oxidized and Reduced States. *Phys. Chem. Chem. Phys.* **2000**, *2*, 4477–4483.

(49) Adler, S. B.; Smith, J. W.; Reimer, J. A. Dynamic Monte Carlo Simulation of Spin-lattice Relaxation of Quadrupolar Nuclei in Solids. Oxygen-17 in Yttria-doped Ceria. *J. Chem. Phys.* **1993**, *98*, 7613–7620.

(50) Viefhaus, T.; Bolse, T.; Müller, K. Oxygen Ion Dynamics in Yttria-Stabilized Zirconia as Evaluated by Solid-State 17O NMR Spectroscopy. *Solid State Ionics* **2006**, *177*, 3063–3068.

(51) Abragam, A. *The Principles of Nuclear Magnetism*; Oxford University Press: Oxford, 1998.

(52) Indris, S.; Heitjans, P.; Uecker, R.; Roling, B. Li Ion Dynamics in a $LiAlO_2$ Single Crystal Studied by ^{7}Li NMR Spectroscopy and Conductivity Measurements. *The Journal of Physical Chemistry C* **2012**, *116*, 14243–14247.

(53) Andrew, E. R.; Jasinski, A. Nuclear Magnetic Resonance Spectra of Rapidly-Rotated Solids Containing Reorienting Molecular Groups. *J. Phys. C: Solid State Phys.* **1971**, *4*, 391.

(54) Hardcastle, F. D.; Wachs, I. E.; Eckert, H.; Jefferson, D. A. Vanadium(V) Environments in Bismuth Vanadates: A Structural Investigation Using Raman Spectroscopy and Solid State 51V NMR. *Journal of Solid State Chemistry* **1991**, *90*, 194–210.

(55) Abrahams, I.; Bush, A. J.; Krok, F.; Hawkes, G. E.; Sales, K. D.; Thornton, P.; Bogusz, W. Effects of Preparation Parameters on Oxygen Stoichiometry in Bi4V2O11–δ. *J. Mater. Chem.* **1998**, *8*, 1213–1217.

(56) Jakobsen, H. J.; Bildsøe, H.; Brorson, M.; Gan, Z.; Hung, I. Quantitative Dynamics and Structure for Crystalline Cs2WO4 and KMnO4 Determined from High-Field 17O Variable-Temperature MAS NMR Experiments. *J. Phys. Chem. C* **2014**, *118*, 20639–20646.

(57) Payne, J. L.; Farrell, J. D.; Linsell, A. M.; Johnson, M. R.; Evans, I. R. The Mechanism of Oxide Ion Conductivity in Bismuth Rhenium Oxide, Bi28Re2O49. *Solid State Ionics* **2013**, *244*, 35–39.

(58) Tate, M. L.; Hack, J.; Kuang, X.; McIntyre, G. J.; Withers, R. L.; Johnson, M. R.; Radosavljevic Evans, I. Bi1-xNbxO1.5+x (X=0.0625, 0.12) Fast Ion Conductors: Structures, Stability and Oxide Ion Migration Pathways. *Journal of Solid State Chemistry* **2015**, *225*, 383–390.

TOC figure

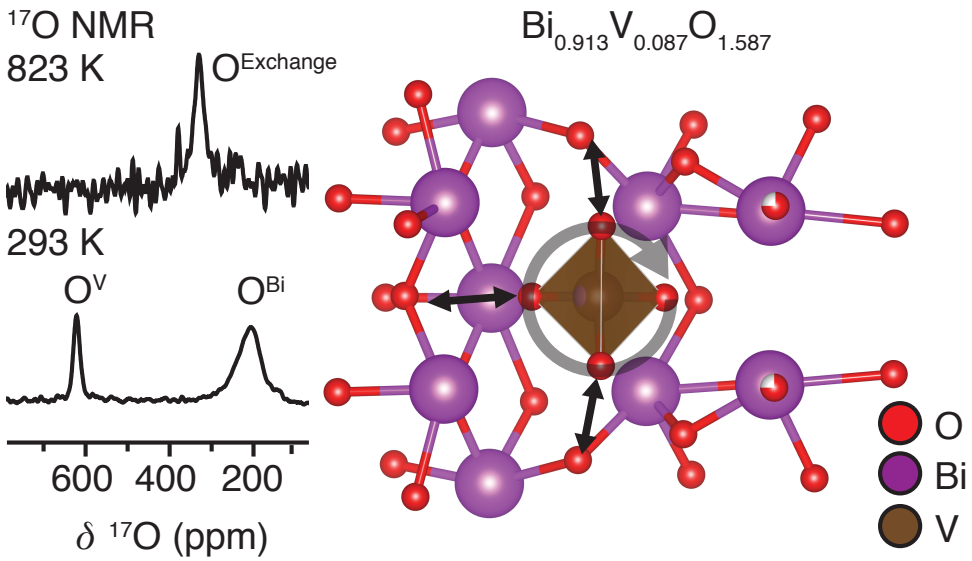
17O NMR
823 K
OExchange
293 K
OV
OBi
600 400 200
δ 17O (ppm)
Bi0.913V0.087O1.587
O
Bi
V